Electric field induced hyperfine level-crossings in (nD)Cs at two-step laser excitation: experiment and theory

M. Auzinsh, K. Blushs, R. Ferber, F. Gahbauer, A. Jarmola, and M. Tamanis
Department of Physics and Institute of Atomic Physics and Spectroscopy, University of Latvia, 19 Rainis Blvd., LV-1586 Riga, Latvia
(Dated: October 31, 2005)

The pure electric field level-crossing of m_F Zeeman sublevels of hyperfine F levels at two-step laser excitation was described theoretically and studied experimentally for the $n\mathrm{D}_{3/2}$ states in Cs with $n = 7$, 9 and 10, by applying a diode laser in the first $6\mathrm{S}_{1/2} \rightarrow 6\mathrm{P}_{3/2}$ step and a diode or dye laser for the second $6\mathrm{P}_{3/2} \rightarrow n\mathrm{D}_{3/2}$ step. Level-crossing resonance signals were observed in the $n\mathrm{D}_{3/2} \rightarrow 6\mathrm{P}_{1/2}$ fluorescence. A theoretical model was developed to describe quantitatively the resonance signals by correlation analysis of the optical Bloch equations in the case when an atom simultaneously interacts with two laser fields in the presence of an external dc electric field. The simulations described well the experimental signals. The tensor polarizabilities α_2 (in a_0^3) were determined to be $7.45(20) \times 10^4$ for the $7\mathrm{D}_{3/2}$ state and $1.183(35) \times 10^6$ for the $9\mathrm{D}_{3/2}$ state; a well established α_2 value for $10\mathrm{D}_{3/2}$ was used to calibrate the electric field. The α_2 value for the $7\mathrm{D}_{3/2}$ state differed by ca. 15% from the existing experimentally measured value.

PACS numbers: 32.10.Dk; 32.60.+i; 32.80.Bx
Keywords: Level-crossing spectroscopy; Hyperfine manifold; Cesium; Two-step laser excitation; Polarizability

I. INTRODUCTION

The first experimental demonstration of crossings of certain magnetic (m_F) components of hyperfine structure (hfs) levels F at non-zero electric field $\mathcal{E}$ was reported in 1966 in a paper by Khadjavi, Happer and Lurio [1]. In this work, the authors observed the Stark effect in the second excited state of the alkali metal atoms ^{85,87}Rb ($6\mathrm{P}_{3/2}$) and ^{133}Cs ($7\mathrm{P}_{3/2}$). Using resonant excitation from a gas-discharge lamp, they observed resonances at the level-crossing positions in the fluorescence signals from single-step broad-line light excitation. Such a method of Stark level-crossing spectroscopy was applied by the same authors to determine experimentally the tensor polarizabilities α_2 in these states, as well as to determine α_2 in ^{39}K($5\mathrm{P}_{3/2}$) [2, 3]. Later on, however, it became more popular to vary the magnetic field in the presence of a constant electric field. This way of inducing level-crossings was preferred, perhaps because magnetic fields were easier to produce and control. Such techniques were used to measure the tensor polarizabilities α_2 of alkali atoms by Svanberg and co-authors (see [4, 5, 6, 7] and references therein). In particular, this method was used in a two-step excitation with a radio-frequency discharge lamp and a narrow-width dye laser [5, 6, 7]. The development of narrow line-width lasers enabled Stark shifts to be measured directly [8] by scanning the electric field at a fixed laser frequency. Both methods made it possible to determine a large number of excited S and D state scalar and tensor polarizabilities of Rb and Cs, achieving an accuracy of some 5% (see [9] for a review). The use of electro-optically modulated laser radiation allowed Xia and co-authors [10] to measure the scalar and tensor polarizabilities of $(10 - 13)\mathrm{D}_{3/2,5/2}$ states of Cs with an accuracy better than 0.3%, which is better than for any other atomic state.

Thus, to our knowledge there has been no experimental observation of purely electric field level-crossing resonances of m_F hfs levels at two-step, or any multi-step, laser excitation. At the same time, no detailed theoretical descriptions of the expected signals at two-step excitation had been reported in the literature until now.

The purpose of the present investigation was (i) to observe the Stark effect induced level-crossing resonances at two-step laser excitation; (ii) to develop a proper theoretical description based on the optical Bloch equations for radiation fields with finite spectral widths [11]; and (iii) to study experimentally the tensor polarizabilities α_2 for the $n\mathrm{D}_{3/2}$ states of Cs atoms which were accessible with laser sources at our disposal, namely the states with $n = 7, 9$, and 10. The $7\mathrm{D}_{3/2}$ state was of particular interest because of a considerable discrepancy between the only known measured value for the polarizability α_2 [12] and its theoretical estimate given in [13]. At the same time, the α_2 value for the $10\mathrm{D}_{3/2}$ Cs state was measured with unprecedented accuracy of 0.1% [10] and remarkably agreed, within 0.25%, with its calculated counterpart in [13]. As a result, we used the signal from the $10\mathrm{D}_{3/2}$ state to calibrate the electric field produced in our Cs cell. A measurement of both states in the same experimental arrangement allowed us to measure the polarizability in the $7\mathrm{D}_{3/2}$ state as well as in the $9\mathrm{D}_{3/2}$ state with greater confidence. Furthermore, Stark effect studies in highly excited Cs states were particularly interesting, as Cs might be useful as a tracer gas to image electric fields [14] at room temperature, or even lower temperatures.

II. EXPERIMENT

A. Method

In our experiment, we detected the resonance signals caused by hfs level-crossings in an external dc electric field when several m_F Zeeman sublevels of hfs levels were coherently excited. Figure 1 illustrates the crossing points of the hyperfine sublevels in the (7,9,10)$D_{3/2}$ states. The stepwise two-laser excitation $6S_{1/2} \rightarrow 6P_{3/2} \rightarrow nD_{3/2}$ of the $7D_{3/2}$, $9D_{3/2}$ and $10D_{3/2}$ levels of atomic cesium was followed by the $nD_{3/2} \rightarrow 6P_{1/2}$ fluorescence, as shown in Fig. 2. The fluorescence intensity signal as a function of the electric field strength is expected to contain resonances at positions corresponding to the m_F level-crossings. To predict the resonance positions, we computed the energy level splitting diagram in the presence of an electric field for hfs levels in the $nD_{3/2}$ states of Cs under study (see Fig. 1) using α_2 values calculated by Wijngaarden and Li [13]. We performed this calculation, whose results are shown in Fig. 1 by diagonalizing the hfs and Stark interaction Hamiltonian written in an uncoupled basis [15]. The values for the hfs constant A were taken from the review of Arimondo and collaborators [16], in which the following values were given: $A = 7.4(2)$ MHz for $7D_{3/2}$ as measured in [7], $A = 2.35(4)$ MHz for $9D_{3/2}$, and $A = 1.51(2)$ MHz for $10D_{3/2}$ as measured in [17, 18]. To our knowledge, no other experimental data of hfs constants for these states of Cs were present in literature. Values for the hfs constant B were not reported and were assumed to be small.

As seen in Fig. 1, two crossings were predicted in the experimentally available electric field range: one crossing within the $F = 4$ manifold with $\Delta m_F = \pm 1$ and ± 2 and a second $\Delta m_F = \pm 2$ crossing between the $m_F = \pm 5$ sublevels of the $F = 5$ level and the $m_F = \pm 3$ sublevel of the $F = 4$ level. When the atoms were excited with linearly polarized light, and linearly polarized fluorescence light was observed, resonances were expected at the electric field values corresponding the the level-crossings with $\Delta m_F = \pm 2$ [19, 20].

B. Experimental details

The schematic diagram of the experiment is depicted in Fig. 3. In our experiment, cesium vapor was produced in a sealed glass cell kept at room temperature. An electric field up to $\mathcal{E} = 2400$ V/cm was applied via transparent Stark electrodes located inside the cell. Therefore, fluorescence light could be observed in the direction of the electric field. The electrodes were separated by two ceramic spacer-rods, which had a diameter of 2.5 mm. The transparent electrodes were produced by depositing Indium-Tin-Oxide vapor on two glass plates. High voltage could be applied to these electrodes using two metal rods which protruded through the glass cell wall. High-temperature conducting silver paste was used to provide a contact between the electrodes and the metal rods.

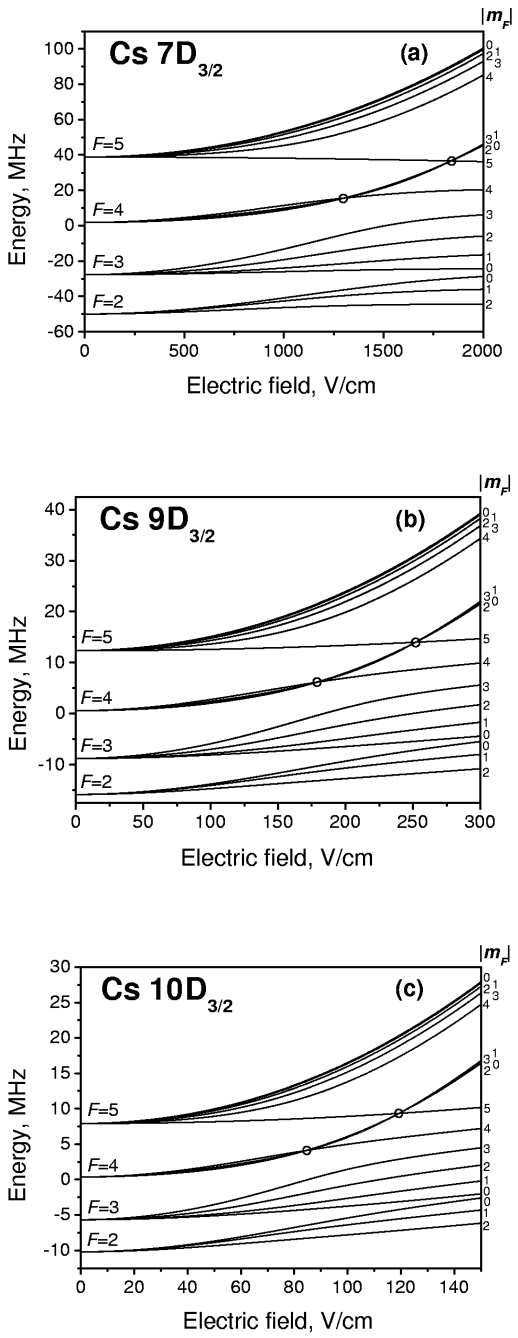

FIG. 1: Hyperfine level splitting diagram in an external electric field for the $7D_{3/2}$ (a), $9D_{3/2}$ (b), and $10D_{3/2}$ (c) states of Cs, with zero energy corresponding to the fine structure level energy.

The $7D_{3/2}$, $9D_{3/2}$, and $10D_{3/2}$ states of cesium were studied using two-step laser excitation (see Fig. 2). For the first step, 852.1 nm radiation of the diode laser (LD-0850-100sm laser diode) was used to excite the $6P_{3/2}$ state. The first laser was linearly polarized with polar-

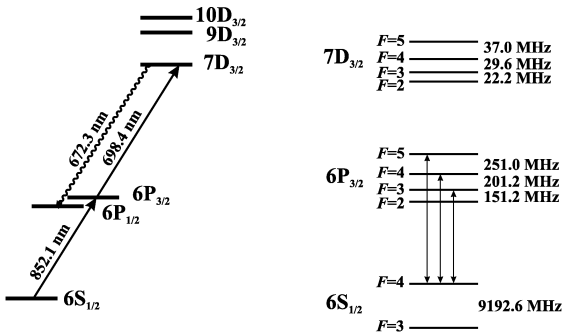

FIG. 2: Cesium energy-level scheme with hfs level spacings shown on the right of the figure.

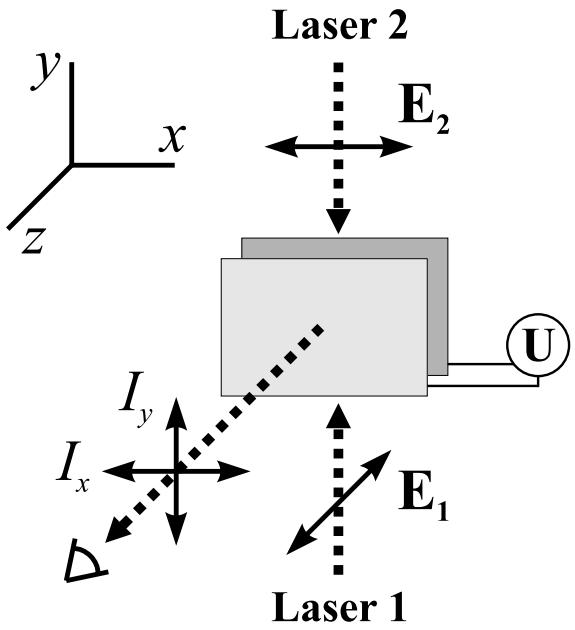

FIG. 3: Schematic diagram of the experiment. The electrodes produced an electric field along the z-axis, which was also parallel to the polarization vector of the first laser $\mathbf{E}_1$ and the observation direction. The observed LIF intensity I_x or I_y polarization direction could be chosen by linear polarizers.

ization vector $\mathbf{E}_1$ along the external dc electric field $\mathcal{E}$ direction ($\mathcal{E} \parallel \mathbf{z}$). Radiation from the second laser, polarized as $\mathbf{E}_2 \parallel \mathbf{x}$, was sent in a counter-propagating direction to induce either the $6P_{3/2} \rightarrow 7D_{3/2}$ transition at 698.4 nm using a Hitachi HL6738MG laser diode or the $6P_{3/2} \rightarrow 9D_{3/2}$ transition at 584.8 nm and the $6P_{3/2} \rightarrow 10D_{3/2}$ transition at 563.7 nm using a Coherent CR699-21 ring dye laser with Rodamin 6G dye. The dye laser was pumped by a Spectra-Physics 171 argon ion laser operating at the 514.5 nm line. The laser induced fluorescence (LIF) $nD_{3/2} \rightarrow 6P_{1/2}$ was observed at 672.3 nm, 566.4 nm, and 546.6 nm, for $n = 7, 9$, and 10, respectively. Before being observed, the LIF passed through a linear polarizer. The observation direction was along the z-axis. Hence, we could observe the LIF intensity components I_x and I_y (see Fig. 3), which were polarized parallel and perpendicular to $\mathbf{E}_2$, respectively.

In order to excite the cesium atoms from the ground state hyperfine level with total angular momentum quantum number $F = 4$ to all allowed $6P_{3/2}$ state hyperfine levels $F = 3, 4, 5$, the first laser was operated in a multimode regime. When the second laser was the diode laser, we applied a 10-20 Hz saw-tooth signal to the piezoelectric crystal mounted to its grating in order to jitter its output frequency over a range of 1.2 GHz. The dye laser was operated in a single-mode regime. To avoid optical pumping, neutral density filters were used to reduce the dye laser intensity. The power of the diode and dye lasers were not more than 3 and 10 mW, respectively. The laser beams had a diameter of approximately 1 mm. The frequency of both lasers was adjusted to maximize the observed fluorescence intensities at the beginning of each measurement.

The LIF was focused by means of a two-lens system onto the entrance slit of a model MDR-3 monochromator with 1.3 nm/mm inverse dispersion and detected with a model FEU-79 photomultiplier tube, which was operated in photon counting mode. The intensities I_x and I_y of the LIF were detected as a function of $\mathcal{E}$. During the experiment, the high voltage between the electrodes was scanned continuously. The photon counts were accumulated during one second intervals and recorded on a PC together with the electrode voltage using a voltage divider. Signals were accumulated during more than 10 scans of approximately 100 s duration, binned and averaged. We could adjust for the delay between the voltage that was recorded and the actual voltage during the integration interval by comparing the results recorded with rising and falling voltages.

C. Results

The measured relative fluorescence intensity was plotted as a function of electric field strength in Figs. 4–6. The measured signals were represented by dots, whereas solid lines were plotted to represent the results of simulations. The model on which these simulations were based was described in Section 3 of this paper. The error bars reflected the statistical variation in each bin after the scans were averaged. We labeled the experimental geometry as zyx or zyy: the first letter z denoted the orientation of the polarization of the first laser $\mathbf{E}_1$ (see Fig. 3), the second letter y denoted the orientation of $\mathbf{E}_2$, and the third letter x or y denoted the direction of LIF polarization that we observed.

The measurements for the $10D_{3/2}$ state were plotted in Fig. 4. Since the tensor polarizability α_2 for the $10D_{3/2}$ state was known far better than for the other states [10], we used the data in Fig. 4 to calibrate the voltage. In Fig. 4, the voltage scale was left uncalibrated to illustrate

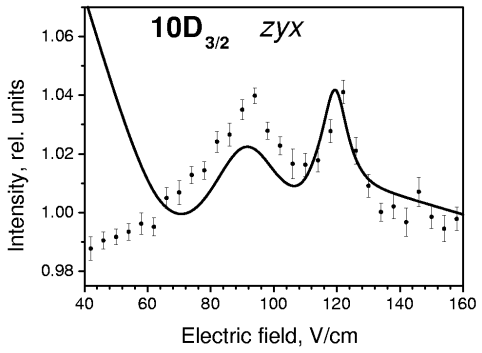

FIG. 4: Fluorescence vs. electric field for the $10D_{3/2}$ state, zyx geometry. Dots, measurement; solid line, calculation. The voltage scale before calibration was plotted.

the precision with which the electrode spacing was known before calibration. To simulate the results, we used the hyperfine constant A and experimentally determined tensor polarizability α_2 shown in Table I. By comparing the position of the second peak (corresponding to the F=4 to F=5 crossing) in our measured curve with the peak position of the calculated curve, we determined that the voltage scale had to be corrected by 2%.

The results for the $9D_{3/2}$ and $7D_{3/2}$ states were plotted in Figs. 5 and 6, respectively. The voltage scales in Figs. 5 and 6 have been adjusted using the scaling factor obtained from the calibration with the $10D_{3/2}$ signal in Fig. 4. The solid lines in Figs. 5 and 6 represented the result of calculations, which were performed using the hyperfine constant A from Table I and a tensor polarizability α_2 adjusted so that the peak positions in the simulations and measured data matched. To illustrate the sensitivity of our method, we included in Fig. 6 as a dashed line the results of a calculation using the previously measured α_2 values shown in Table I.

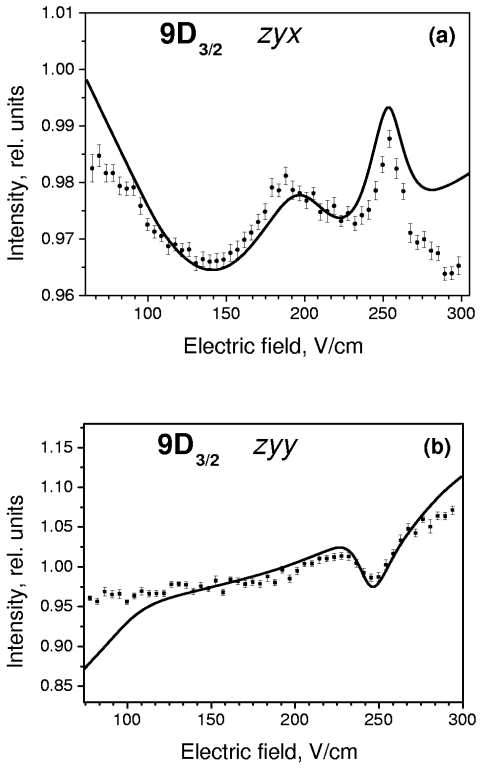

FIG. 5: Fluorescence vs. electric field for the $9D_{3/2}$ state, zyx geometry (a) and zyy (b). Dots, measurements; solid line, calculation. The voltage scale was calibrated using data from Fig. 4.

III. THEORETICAL MODEL

A. Outline of the model

In the experiment described above, atoms strongly interacted with radiation simultaneously produced by two lasers. Nonlinear interactions can cause shifts of the magnetic levels in the laser field [21], and as a result, shifts of the level-crossing positions. The theoretical description of our experiment was further complicated by the fact, that in order to excite coherently magnetic sublevels that were split in an external field, we used the lasers that generated a rather broad profile of radiation. In this situation, a model that was able to describe signals quantitatively was essential in order to analyze the obtained signals and to be able to deduce atomic constants from these signals.

In the present study, such a model was elaborated on the basis of an approach that we developed for the rate equations for Zeeman coherences in the case where atoms were excited by one partially coherent optical field [11].

In this paper, we extended this approach to the case when an atom interacts with two laser fields simultaneously in presence of an external dc electric field $\mathcal{E}$. We assumed that the atomic center of mass moved classically, which meant that the description of the dipole interaction of the atom with the laser fields could assume a classically moving atom that was excited at the internal transitions. In this case the internal atomic dynamics could be described by the semiclassical atomic density matrix ρ, which parametrically depended on the classical coordinates of the atomic center of mass.

We considered the absorption of the first laser's radiation as the atoms were excited from the atomic ground state denoted by g to the intermediate state denoted by e. Then a second laser excited the atoms further from the e state to the final state f. The direct transition $g \leftrightarrow f$ was forbidden in the dipole approximation. In our particular case (see Fig. 2), the ground state of the Cs atom consisted of two hfs levels $F_g = 3$ and $F_g = 4$. Each of these

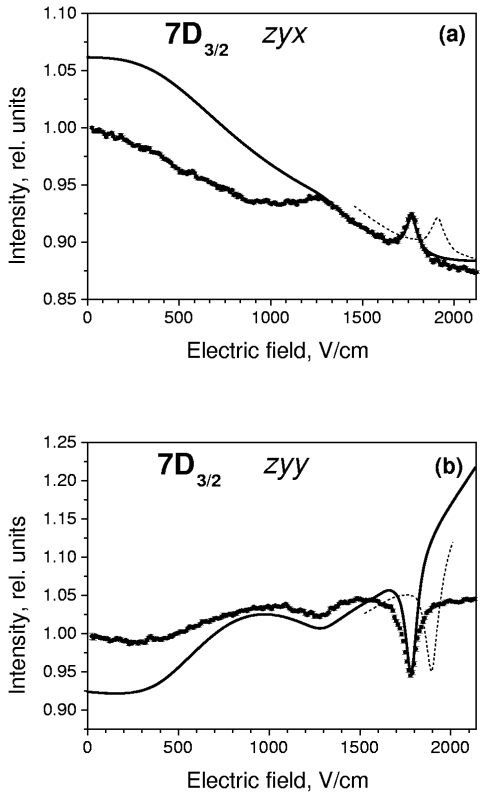

FIG. 6: Fluorescence vs. electric field for the $7D_{3/2}$ state, zyx geometry (a) and zyy (b). Dots, measurements; solid line, calculation; dashed line, calculation using the tensor polarizability value from [12]. The voltage scale was calibrated using data from Fig. 4.

hfs levels in turn consisted of $2F_g+1$ magnetic sublevels, denoted by g_i in what follows. The intermediate state in our experiment was the $6P_{3/2}$ state of the Cs atom. It consisted of four hyperfine levels with $F_e = 2, 3, 4$ and 5 and the corresponding number of magnetic sublevels, denoted as e_i. Finally, the atomic level that was excited by the second laser was the $nD_{3/2}$ state, which again consisted of hyperfine levels with $F_f = 2, 3, 4$ and 5. We denoted the magnetic sublevels of these states as f_i.

To simulate the observed signals, we had to take into account that the external electric field was strong enough to break partially the hyperfine interaction between electronic angular momentum of the atom and the nuclear spin. As a result (see Fig. 1) the magnetic sublevel energies in the external dc electric field did not depend quadratically on the electric field strength any more. This dependence could be obtained only by diagonalizing the full Hamilton matrix. The partial decoupling of the electronic angular momentum and nuclear spin altered also the dipole transition probabilities between the magnetic sublevels of the atoms belonging to the different fine structure levels. This decoupling was taken into account in the simulation of the experimental signals.

With the above assumptions, we were able to develop a model, described below, to calculate the observed level-crossing signals in our experiment.

B. Optical Bloch equations

We started our analysis from the optical Bloch equations (OBEs) for the density matrix elements $\rho_{g_ig_j}$, $\rho_{g_ie_j}$, $\rho_{g_if_j}$, $\rho_{e_ig_j}$, $\rho_{e_ie_j}$, $\rho_{e_if_j}$, $\rho_{f_ig_j}$, $\rho_{f_ie_j}$, and $\rho_{f_if_j}$. In writing OBEs (see for example [22]),

$$i\hbar\frac{\partial\rho}{\partial t} = \left[\widehat{H},\widetilde{\rho}\right] + i\hbar\widehat{R}\rho, \tag{1}$$

we considered the relaxation $\widehat{R}$ operator to include spontaneous emission and transit relaxation due to the thermal motion of atoms into and out of the laser beam. We also assumed that different velocity groups of the thermally moving atoms did not interact – the density of atoms was sufficiently low. In this case the relaxation matrix was:

$$\begin{aligned}
\widehat{R}\rho_{g_ig_j} &= \sum_{e_ie_j}\Gamma^{e_ie_j}_{g_ig_j}\rho_{e_ie_j} - \gamma\rho_{g_ig_j} + \lambda\delta_{g_i,g_j},\\
\widehat{R}\rho_{g_ie_j} &= -\frac{\Gamma_e}{2}\rho_{g_ie_j} - \gamma\rho_{g_ie_j},\\
\widehat{R}\rho_{g_if_j} &= -\frac{\Gamma_f}{2}\rho_{g_if_j} - \gamma\rho_{g_if_j},\\
\widehat{R}\rho_{e_ig_j} &= -\frac{\Gamma_e}{2}\rho_{e_ig_j} - \gamma\rho_{e_ig_j},\\
\widehat{R}\rho_{e_ie_j} &= -\Gamma_e\rho_{e_ie_j} + \sum_{f_if_j}\Gamma^{f_if_j}_{e_ie_j}\rho_{f_if_j} - \gamma\rho_{e_ie_j},\\
\widehat{R}\rho_{e_if_j} &= -\left(\frac{\Gamma_e}{2}+\frac{\Gamma_f}{2}\right)\rho_{e_if_j} - \gamma\rho_{e_if_j},\\
\widehat{R}\rho_{f_ig_j} &= -\frac{\Gamma_f}{2}\rho_{f_ig_j} - \gamma\rho_{f_ig_j},\\
\widehat{R}\rho_{f_ie_j} &= -\left(\frac{\Gamma_e}{2}+\frac{\Gamma_f}{2}\right)\rho_{f_ie_j} - \gamma\rho_{f_ie_j},\\
\widehat{R}\rho_{f_if_j} &= -\Gamma_f\rho_{f_if_j} - \gamma\rho_{f_if_j},
\end{aligned} \tag{2}$$

where γ and λ were the transit relaxation rates. The quantity $\lambda\delta_{g_i,g_j}$ described the process in which "fresh" atoms were moving into the laser beam, and γ described the rate at which atoms were leaving the interaction region. Γ_e was the total spontaneous relaxation rate from level e, Γ_f was the total spontaneous relaxation rate from level f, $\Gamma^{e_ie_j}_{g_ig_j}$ described the spontaneous relaxation from $\rho_{e_ie_j}$ to $\rho_{g_ig_j}$, $\Gamma^{f_if_j}_{e_ie_j}$ described the spontaneous relaxation from $\rho_{f_if_j}$ to $\rho_{e_ie_j}$. The explicit forms of these rate coefficients were calculated on the basis of angular momentum algebra and can be found in [23].

The Hamiltonian $\widehat{H} = \widehat{H}_0 + \widehat{V}$ included the unperturbed atomic Hamiltonian $\widehat{H}_0$ and the dipole interaction

operator $\widehat{V} = -\widehat{\mathbf{d}} \cdot \mathbf{E}(t)$, where $\widehat{\mathbf{d}}$ was the electric dipole operator. The exciting light was described classically by two uncorrelated fluctuating electric fields $\mathbf{E_1}$ and $\mathbf{E_2}$ of definite polarizations $\mathbf{e}_1$ and $\mathbf{e}_2$:

$$\begin{aligned} \mathbf{E}(t) &= \mathbf{E}_1(t) + \mathbf{E}_2(t), \\ \mathbf{E}_i(t) &= \varepsilon_i(t)\,\mathbf{e}_i + \varepsilon_i^*(t)\,\mathbf{e}_i^*, \\ \varepsilon_i(t) &= |\varepsilon_{\overline{\omega}_i}| \exp\left[-i\Phi_i(t) - i\left(\overline{\omega}_i \mp \mathbf{k}_{\overline{\omega}_i}\mathbf{v}\right)t\right], \end{aligned} \tag{3}$$

with the center frequency of the radiation spectrum $\overline{\omega}_i$ and the fluctuating phase $\Phi_i(t)$. The lineshape of the exciting light was assumed to be Lorentzian with FWHM $\Delta\omega_i$. Atoms moved with definite velocity $\mathbf{v}$, which gave the shift $\overline{\omega}_i \mp \mathbf{k}_{\overline{\omega}_i}\mathbf{v}$ in the laser frequency that the atom would encounter due to the Doppler effect, where $\mathbf{k}_{\overline{\omega}_i}$ was the wave vector of the exciting light. The minus sign referred to the laser beam that propagated in the positive direction of the y-axis (see Fig. 3) and the plus sign to the counterpropagating laser beam.

Writing OBEs explicitly for the density matrix elements ρ_{ij}, we obtained:

$$\begin{aligned} \frac{\partial \rho_{ij}}{\partial t} &= -\frac{i}{\hbar}\left[\widehat{H}, \rho_{ij}\right] + \widehat{R}\rho_{ij} = \\ &= -\frac{i}{\hbar}\left[\widehat{H}_0, \rho_{ij}\right] + \frac{i}{\hbar}\left[\widehat{\mathbf{d}} \cdot \mathbf{E}(t), \rho_{ij}\right] + \widehat{R}\rho_{ij} = \\ &= -i\omega_{ij}\rho_{ij} + \frac{i}{\hbar}\mathbf{E}(t)\sum_k \left(\mathbf{d}_{ik} \cdot \rho_{kj} - \rho_{ik} \cdot \mathbf{d}_{kj}\right) + \widehat{R}\rho_{ij}, \end{aligned} \tag{4}$$

where $\omega_{ij} = \omega_i - \omega_j$ denoted the splitting of the levels i and j and $\mathbf{d}_{ik} \equiv \langle i|\mathbf{d}|k\rangle$. By choosing the quantization axis (the z-axis) to be parallel to the static electric field $\mathcal{E}$, all the explicit dependence of the density matrix on the static electric field $\mathcal{E}$ was included in the splitting terms ω_{ij}. Implicitly, the density matrix depended on the dc electric field, because this field modified the dipole transition matrix elements by partially decoupling the hyperfine interaction.

In order to simplify the above equation, we did the following: we neglected possible optical excitations of neighboring transitions, that is, we neglected the excitation of the transitions $g \leftrightarrow e$ ($e \leftrightarrow f$) with the second (first) laser, which was tuned to the transition $e \leftrightarrow f$ ($g \leftrightarrow e$). Then, in order to eliminate fast oscillations with optical frequencies $\overline{\omega}_i$, we applied to the optical Bloch equations the rotating wave approximation for multilevel systems as developed in [24]:

$$\begin{aligned} \rho_{ge} &= \widetilde{\rho}_{ge}\, e^{i\left(\overline{\omega}_1 - \mathbf{k}_{\overline{\omega}_1}\boldsymbol{v}\right)t + i\Phi_1(t)} = \rho_{eg}^*, \\ \rho_{gf} &= \widetilde{\rho}_{gf}\, e^{i\left(\overline{\omega}_1 + \overline{\omega}_2 - \mathbf{k}_{\overline{\omega}_1}\boldsymbol{v} + \mathbf{k}_{\overline{\omega}_2}\boldsymbol{v}\right)t + i\Phi_1(t) + i\Phi_2(t)} = \rho_{fg}^*, \\ \rho_{ef} &= \widetilde{\rho}_{ef}\, e^{i\left(\overline{\omega}_2 + \mathbf{k}_{\overline{\omega}_2}\boldsymbol{v}\right)t + i\Phi_2(t)} = \rho_{fe}^*. \end{aligned} \tag{5}$$

C. Laser radiation fluctuations

In the optical Bloch equations we distinguished Zeeman coherences that corresponded to the density matrix elements $\widetilde{\rho}_{gg}$, $\widetilde{\rho}_{ee}$, $\widetilde{\rho}_{ff}$ and optical coherences that corresponded to the density matrix elements $\widetilde{\rho}_{ef}$, $\widetilde{\rho}_{fe}$, $\widetilde{\rho}_{ge}$, $\widetilde{\rho}_{eg}$. As a result we arrived at a system of stochastic differential equations (4) with stochastic variables $\Phi_i(t)$. We simplified this system by applying the "decorrelation approach" [25].

In the experiment we observed signals that were averaged over time intervals that were large in comparison with the characteristic phase-fluctuation time of the excitation-light source. Therefore we needed to perform a statistical averaging of the above equations. In order to do that, we solved the equations for optical coherences and then took a formal statistical average over the fluctuating phases (for details see [11]). Additionally we assumed that both lasers were uncorrelated and that optical coherences $\widetilde{\rho}_{ef}, \widetilde{\rho}_{fe}$ ($\widetilde{\rho}_{ge}, \widetilde{\rho}_{eg}$) were independent of the fluctuations of the first (second) laser, which was tuned to the transition $g \leftrightarrow e$ ($e \leftrightarrow f$). Then we applied the "decorrelation approximation" (see [11] and references cited therein):

$$\left\langle \rho_{ij}\left(t'\right) e^{\pm i\left[\Phi(t)-\Phi\left(t'\right)\right]}\right\rangle = \left\langle \rho_{ij}\left(t'\right)\right\rangle \left\langle e^{\pm i\left[\Phi(t)-\Phi\left(t'\right)\right]}\right\rangle . \tag{6}$$

The correlation function $\left\langle e^{\pm i\left[\Phi(t)-\Phi\left(t'\right)\right]}\right\rangle$ was calculated assuming the "phase diffusion" model of the laser radiation for the description of the dynamics of the fluctuating phase [11]. Thus,

$$\left\langle e^{\pm i\left[\Phi(t)-\Phi\left(t'\right)\right]}\right\rangle = e^{-\frac{\triangle\omega}{2}\left(t-t'\right)}. \tag{7}$$

Putting it all together, we arrived at the phase-averaged OBEs (for simplicity we dropped the averaging brackets). In the case of stationary time-independent excitation we obtained

$$\begin{aligned}
\rho_{g_ig_j} &= \frac{i}{\hbar}\frac{\left|\varepsilon_{\overline{\omega}_1}\right|}{\gamma+i\omega_{gigj}}\sum_{e_k}\left(d^{(1)*}_{g_ie_k}\widetilde{\rho}_{e_kg_j}-d^{(1)}_{e_kg_j}\widetilde{\rho}_{g_ie_k}\right)+\\
&\quad+\frac{1}{\gamma+i\omega_{gigj}}\left(\sum_{e_ie_j}\Gamma^{e_ie_j}_{g_ig_j}\rho_{e_ie_j}+\lambda\delta\left(g_i,g_j\right)\right),\\
\widetilde{\rho}_{g_ie_j} &= \frac{i}{\hbar}\frac{1}{\left(\frac{\Gamma_e}{2}+\gamma+\frac{\triangle\omega_1}{2}\right)+i\left(\overline{\omega}_1-\mathbf{k}_{\overline{\omega}_1}\boldsymbol{v}+\omega_{giej}\right)}\times\\
&\quad\times\left(\left|\varepsilon_{\overline{\omega}_1}\right|\sum_{e_k}d^{(1)*}_{g_ie_k}\rho_{e_ke_j}-\left|\varepsilon_{\overline{\omega}_1}\right|\sum_{g_k}d^{(1)*}_{g_ke_j}\rho_{g_ig_k}-\left|\varepsilon_{\overline{\omega}_2}\right|\sum_{f_k}d^{(2)}_{f_ke_j}\widetilde{\rho}_{g_if_k}\right),\\
\widetilde{\rho}_{g_if_j} &= \frac{i}{\hbar}\frac{1}{\left(\frac{\Gamma_f}{2}+\gamma+\frac{\triangle\omega_1}{2}+\frac{\triangle\omega_2}{2}\right)+i\left(\overline{\omega}_1+\overline{\omega}_2-\mathbf{k}_{\overline{\omega}_1}\boldsymbol{v}+\mathbf{k}_{\overline{\omega}_2}\boldsymbol{v}+\omega_{g_if_j}\right)}\times\\
&\quad\times\sum_{e_k}\left(\left|\varepsilon_{\overline{\omega}_1}\right|d^{(1)*}_{g_ie_k}\widetilde{\rho}_{e_kf_j}-\left|\varepsilon_{\overline{\omega}_2}\right|d^{(2)*}_{e_kf_j}\widetilde{\rho}_{g_ie_k}\right),\\
\widetilde{\rho}_{e_ig_j} &= \frac{i}{\hbar}\frac{1}{\left(\frac{\Gamma_e}{2}+\gamma+\frac{\triangle\omega_1}{2}\right)-i\left(\overline{\omega}_1-\mathbf{k}_{\overline{\omega}_1}\boldsymbol{v}-\omega_{e_ig_j}\right)}\times\\
&\quad\times\left(\left|\varepsilon_{\overline{\omega}_1}\right|\sum_{g_k}d^{(1)}_{e_ig_k}\rho_{g_kg_j}-\left|\varepsilon_{\overline{\omega}_1}\right|\sum_{e_k}d^{(1)}_{e_kg_j}\rho_{e_ie_k}+\left|\varepsilon_{\overline{\omega}_2}\right|\sum_{f_k}d^{(2)*}_{e_if_k}\widetilde{\rho}_{f_kg_j}\right),\\
\rho_{e_ie_j} &= \frac{i}{\hbar}\frac{\left|\varepsilon_{\overline{\omega}_1}\right|}{\left(\Gamma_e+\gamma\right)+i\omega_{e_ie_j}}\sum_{g_k}\left(d^{(1)}_{e_ig_k}\widetilde{\rho}_{g_ke_j}-d^{(1)*}_{g_ke_j}\widetilde{\rho}_{e_ig_k}\right)+\\
&\quad+\frac{i}{\hbar}\frac{\left|\varepsilon_{\overline{\omega}_2}\right|}{\left(\Gamma_e+\gamma\right)+i\omega_{e_ie_j}}\sum_{f_k}\left(d^{(2)*}_{e_if_k}\widetilde{\rho}_{f_ke_j}-d^{(2)}_{f_ke_j}\widetilde{\rho}_{e_if_k}\right)+\\
&\quad+\frac{1}{\left(\Gamma_e+\gamma\right)+i\omega_{e_ie_j}}\sum_{f_if_j}\Gamma^{f_if_j}_{e_ie_j}\rho_{f_if_j},\\
\widetilde{\rho}_{e_if_j} &= \frac{i}{\hbar}\frac{1}{\left(\frac{\Gamma_e}{2}+\frac{\Gamma_f}{2}+\gamma+\frac{\triangle\omega_2}{2}\right)+i\left(\overline{\omega}_2-\mathbf{k}_{\overline{\omega}_2}\boldsymbol{v}+\omega_{e_if_j}\right)}\times\\
&\quad\times\left(\left|\varepsilon_{\overline{\omega}_2}\right|\sum_{f_k}d^{(2)*}_{e_if_k}\rho_{f_kf_j}-\left|\varepsilon_{\overline{\omega}_2}\right|\sum_{e_k}d^{(2)*}_{e_kf_j}\rho_{e_ie_k}+\left|\varepsilon_{\overline{\omega}_1}\right|\sum_{g_k}d^{(1)}_{e_ig_k}\widetilde{\rho}_{g_kf_j}\right),
\end{aligned} \tag{8}$$

$$\widetilde{\rho}_{f_i g_j} = \frac{i}{\hbar} \frac{1}{\left(\frac{\Gamma_f}{2} + \gamma + \frac{\triangle\omega_1}{2} + \frac{\triangle\omega_2}{2}\right) - i\left(\overline{\omega}_1 + \overline{\omega}_2 - \overrightarrow{k_{\overline{\omega}_1}}\overrightarrow{v} - \overrightarrow{k_{\overline{\omega}_2}}\overrightarrow{v} - \omega_{f_i g_j}\right)} \times$$
$$\times \sum_{e_k} \left(|\varepsilon_{\overline{\omega}_2}|\, d^{(2)}_{f_i e_k} \widetilde{\rho}_{e_k g_j} - |\varepsilon_{\overline{\omega}_1}|\, d^{(1)}_{e_k g_j} \widetilde{\rho}_{f_i e_k} \right),$$

$$\widetilde{\rho}_{f_i e_j} = \frac{i}{\hbar} \frac{1}{\left(\frac{\Gamma_e}{2} + \frac{\Gamma_f}{2} + \gamma + \frac{\triangle\omega_2}{2}\right) - i\left(\overline{\omega}_2 - \mathbf{k}_{\overline{\omega}_2}\boldsymbol{v} - \omega_{f_i e_j}\right)} \times$$
$$\times \left(|\varepsilon_{\overline{\omega}_2}| \sum_{e_k} d^{(2)}_{f_i e_k} \rho_{e_k e_j} - |\varepsilon_{\overline{\omega}_2}| \sum_{f_k} d^{(2)}_{f_k e_j} \rho_{f_i f_k} - |\varepsilon_{\overline{\omega}_1}| \sum_{g_k} d^{(1)*}_{g_k e_j} \widetilde{\rho}_{f_i g_k} \right),$$

$$\rho_{f_i f_j} = \frac{i}{\hbar} \frac{|\varepsilon_{\overline{\omega}_2}|}{(\Gamma_f + \gamma) + i\omega_{f_i f_j}} \sum_{e_k} \left(d^{(2)}_{f_i e_k} \widetilde{\rho}_{e_k f_j} - d^{(2)*}_{e_k f_j} \widetilde{\rho}_{f_i e_k} \right).$$

This system of equations was the one that we solved in order to simulate the observed signals. When the density matrix for the final state was calculated, we obtained the fluorescence intensities with a specific polarization along the unit vector $\mathbf{e}$ as [23, 26, 27]:

$$I(\mathbf{e}) = \widetilde{I}_0 \sum_{g_i, f_i, f_j} d^{(ob)*}_{g_i f_j} d^{(ob)}_{e_i g_i} \rho_{f_i f_j}, \qquad (9)$$

where $\widetilde{I}_0$ was a proportionality coefficient and the matrix element $d^{(ob)}_{g_i f_j} = \langle g_i | \mathbf{d} \cdot \mathbf{e} | f_j \rangle$ contained the polarization vector $\mathbf{e}$ of the light which was detected, i.e. along the x- or y-axis.

IV. ANALYSIS AND DISCUSSION

The theoretical model discussed above was used to simulate our experiment, and the results of the simulations were plotted together with the results of our measurements in Fig. 4–6 as described in Section 2. Since the precise shape of the level-crossing signal depended on various parameters that were beyond our ability to control precisely, these parameters were adjusted in the calculation. The parameters that we adjusted were the Rabi frequencies of the transitions, the laser radiation spectral widths, and the detuning of the laser radiation relative to the exact transition frequencies. In addition, the background was left as an adjustable parameter. The generally good agreement between the calculation and the measurement, except at electric fields far below and above the level-crossing points, validated the theoretical approach described in Section 3.

The positions of the resonances depended on the points where energy levels crossed (see Fig. 1). These, in turn, depended on the values of the hyperfine constants A and B, and on the tensor polarizability α_2. We took the hyperfine constants to be sufficiently well determined (see the review by Arimondo and collaborators [16]) to allow us to use our results to make a new measurement of the tensor polarizabilities of the $9D_{3/2}$ and $7D_{3/2}$ states of cesium. Our results were summarized in Table I and compared with the previous measurements of Fredrikson and Svanberg [9] and of Wessel and Cooper [12], and with the theoretical calculations of α_2 of Wijngaarden and Li [13]. We estimated the accuracy of our value for α_2 based on the reproducibility of several measurements and accounted for the uncertainty of the hyperfine constant A and of the tensor polarizability α_2 of the $10D_{3/2}$ state, on which our electric field calibration was based. Furthermore, we included the error in the measurements of the polarizabilities of the $7D_{3/2}$ and $9D_{3/2}$ states introduced by the reported uncertainties in their respective hyperfine constants, A. The largest contributions to our error were the uncertainty in the hyperfine constants and in the electric field calibration, whose contributions were of comparable magnitude.

Our accuracy was competitive or slightly higher than those of previously reported measurements of the tensor polarizabilities for these atomic states. Our results were consistent with the theoretical predictions for α_2 of [13] for the $9D_{3/2}$ state as well as with the previous measurement of [9]. For the $7D_{3/2}$ state, our measurements indicated a value for α_2 that was higher than both the previous measurement of Wessel and Cooper [12] and the theoretical prediction of [13].

V. CONCLUDING REMARKS

The method of detecting pure electric field induced level-crossing signals of m_F Zeeman sublevels of the hy-

TABLE I: Summary of results.

Cesium Atomic State	Hyperfine Constant (MHz)	Tensor Polarizability α_2 This experiment (a_0^3)	Previous experiment (a_0^3)	Theory (a_0^3)
$10D_{3/2}$	1.51(2) [16]	–	$3.4012(36) \times 10^6$ [10]	3.41×10^6 [13]
$9D_{3/2}$	2.35(4) [16]	$1.183(35) \times 10^6$	$1.258(60) \times 10^6$ [9]	1.19×10^6 [13]
$7D_{3/2}$	7.4(2) [16]	$7.45(20) \times 10^4$	$6.6(3) \times 10^4$ [12]	7.04×10^4 [13]

perfine F levels at two-step laser excitation has been applied to determine experimentally the tensor polarizabilities of highly excited atomic states. Conventional laser sources, including diode lasers, with rather broad line contours were sufficient. In the case of crossings between different F sublevels with $\Delta m_F = \pm 2$, the resonance peaks were sufficiently sharp to enable accurate determination of the peak position. At the same time, the fluorescence intensity behavior within a broader electric field range, including additional crossings, together with reliable signal simulations, enhanced the accuracy of the technique.

For this purpose an adequate theoretical description was worked out by extending an approach previously developed for two-level systems [11] to the case of a three-level system. A significant simplification of the optical Bloch equations was achieved by statistically averaging over the fluctuating phases and applying the "decorrelation approximation. Though the problem was more cumbersome with more parameters to be considered, it made it possible to describe satisfactorily the observed signals. What is more, moderate computation times could be achieved by replacing the Doppler distribution with a group of atoms moving at a definite velocity.

The measured tensor polarizability for the higher-n $9D_{3/2}$ state (see Table I) agreed within experimental error with previously measured and calculated values. At the same time the present measured tensor polarizability for the lower-n $7D_{3/2}$ state differed from the previously measured experimental value [12] by ca. 15% while the theoretical prediction of [13] was lower than our measured value by some 5%.

To increase the accuracy and reliability of experimentally measured tensor polarizabilities, it was useful to use the calibration with respect to a level with well established polarizability value. This approach substantially diminished possible errors in the determination of external electric field values.

For the $7D_{3/2}$ and $9D_{3/2}$ states under study, the accuracy of existing hfs constants limited the accuracy of the tensor polarizability measurement which could be achieved by applying electric field induced level-crossing spectroscopy.

VI. ACKNOWLEDGEMENTS

The authors are indebted to Bruce Shore for numerous stimulating discussions. The authors express sincere gratitude to S. Svanberg, E. Arimondo, H. Metcalf, and V. A. Dzuba for sharing useful information, as well as to Janis Alnis for helping to assemble the diode lasers and to Robert Kalendarev for producing the glass cells. We gratefully acknowledge support from the NATO SfP 978029 Optical Field Mapping grant, from the EC 5th Frame Competitive and Sustainable Growth grant G1MA-CT-2002-04063, and from the Latvian State Research Programme funding (grant 1-23/50). K.B., F.G. and A.J. are grateful to the European Social Fund for support.

[1] A. Khadjavi, W. Happer, Jr., A. Lurio, Phys. Rev. Lett. 17, (1966), 463.
[2] A. Khadjavi, A. Lurio, W. Happer, Phys. Rev. 167, (1968) 128.
[3] Robert W. Schmieder, Allen Lurio, W. Happer, Phys. Rev. A 3 (1971) 1209.
[4] S. Svanberg, Phys. Scr. 5 (1972) 132.
[5] G. Belin, L. Holmgren, I. Lindgren, S. Svanberg, Phys. Scr. 12 (1975) 287.
[6] G. Belin, L. Holmgren, S. Svanberg, Phys. Scr. 13 (1976) 351.
[7] G. Belin, L. Holmgren, S. Svanberg, Phys. Scr.14 (1976) 39.
[8] S. Svanberg, P. Tsekeris, W. Happer, Phys. Rev. Lett. 30 (1973) 817.
[9] K. Fredrikson, S. Svanberg, Z. Physik A 281 (1977) 189.
[10] J. Xia, J. Clarke, J. Li, W. A. Wijngaarden, Phys. Rev. A 56, (1997) 5176.
[11] K. Blush, M. Auzinsh, Phys. Rev. A 69 (2004) 063806.
[12] J. E. Wessel and D. Cooper, Phys. Rev. A 35 (1987) 1621.
[13] W. A. Van Wijngaarden and J. Li, J. Quant. Spect. Rad.Tranf. 52 (1994) 555.
[14] M. Auzinsh, L. Jayasinghe, L. Oelke, R. Ferber, N. Shafer-Ray, J. Phys. D (Applied Physics) 34 (2001) 1.
[15] E. B. Aleksandrov, M. P. Chaika, G. I. Khvostenko, Interference of atomic states: in Springer series on atoms and plasmas, Springer, Berlin, 1993.
[16] E. Arimondo, M Inguscio, P. Violino, Rev. Mod. Phys.

49 (1977) 31.
[17] J. S. Deech, R. Luypaert, G. W. Series, J. Phys. B 8 (1975) 1406.
[18] S. Svanberg, P. Tsekeris, Phys. Rev. A 11 (1975) 1125.
[19] J. Alnis, M. Auzinsh, Phys. Rev. A 63 (2001) 023407.
[20] M. P. Auzinsh, R. S. Ferber, J. Chem Phys. 99 (1993) 5742.
[21] W. Happer, Light Propagation and Light Shifts in Optical Pumping Experiments, in: Progress in quantum electronics, vol. 1, pt. 2, Pergamon Press, Oxford, 1970, p. 51.
[22] S. Stenholm. Foundations of laser spectroscopy. in: Wiley series in pure and applied optics,. Wiley, New York, 1984.
[23] M. Auzinsh, R. Ferber, Optical Polarization of Molecules, Cambridge University Press, Cambridge, 2005.
[24] E. Arimondo, Prog. Opt. 35, 257 (1996).
[25] N. G. van Kampen, Phys. Lett. C 24, (1976) 171.
[26] J. P. Barrat, C. Cohen-Tannoudji, J. Phys. Rad. 22 (1961) 329; 443.
[27] M. I. Dyakonov, Sov. Phys. JETP 20 (1965) 1484.